49th AIAA Aerospace Sciences Meeting including the New Horizons Forum and Aerospace Exposition
4 - 7 January 2011, Orlando, Florida
AIAA 2011-1164

New Seeding and Surface Treatment Methods for Particle Image Velocimetry

Adam J. Pierce,* and Frank K. Lu†
University of Texas at Arlington, Arlington, Texas, 76019

PIV systems rely on a combination of seed particles, laser light intensity, and camera positioning to collected velocity data. Careful attention is needed when selecting the appropriate setup configuration for PIV systems. This paper focuses on several areas for improvement in PIV data collection for a compressible turbulent boundary layer study on a flat plate using MVG's. The topics include determining the seed particle surface preparation for a flat plate, and PIV system configuration.

Nomenclature

α	divergence angle
d	laser beam diameter
f	focal length
d_p	particle diameter
ρ_p	particle density
μ	dynamic viscosity
τ	particle relaxation time

I. Introduction

PARTICLE image velocimetry[1] and the related laser lightsheet visualization[2] are now commonly accepted diagnostics techniques. PIV has recently been extended to stereo, tomographic and microscopic implementations. For aerodynamic applications, the high reflectivity of metallic surfaces can be a serious impediment for resolving flow close to such surfaces. An acceptable but complicated technique is to install transparent inserts to allow the laser light to transmit through the material and by absorbed further into the model. Another problem that can arise is seeding. Some of the issues include particle relaxation time, particle density definition, and problems in decelerating high-speed flows by a shock.

This paper addresses these seeding issues and proposes a simple surface treatment for surface reflections. The improvements were tested in a supersonic blowdown tunnel at Mach 2.5 in diagnosing flows past micro vortex generators.[3]

A. Background on Micro Vortex Generators for High-Speed Applications

This boundary layer flow control technique is to distribute an array of micro vortex generators (MVGs), whose height is less than the boundary layer thickness, ahead of the region with adverse flow conditions.[4–42] These MVGs are thought to function similarly to conventional vortex generators in energizing the boundary layer via entrainment of the freestream flow by trailing vortices. The main difference between MVGs and conventional vortex generators is that the former is produces less drag. They have apparently been deployed in practice and appear to be beneficial under certain circumstances, such as the low-speed performance of

*Graduate Research Assistant, Aerodynamics Research Center, Department of Mechanical and Aerospace Engineering. Student Member AIAA.
†Professor and Director, Aerodynamics Research Center, Department of Mechanical and Aerospace Engineering. Associate Fellow AIAA.

a large transport aircraft[23] and proposed for potential application in supersonic inlets[37] and cabin noise reduction.[4] One form of MVG is wedge shaped as depicted in Fig. 1.

In the existing model of the flow past an MVG, beside the horseshoe vortex, a pair of primary and two pairs of secondary trailing vortices are thought to exist. Babinsky and co-workers,[27,29,33] from surface flow visualization, and Lee et al.,[40] from large eddy simulations, suggest that a pair of counter-rotating vortices trails downstream of an MVG. The experiments indicate a small separation zone ahead of the compression zone which creates a very small horseshoe vortex on either side of a region devoid of pigment where a herringbone pattern can be seen. This herringbone pattern, as observed in other three-dimensional flows, is thought to be the result of open separation. This open separation zone is dominated by a pair of large, counter-rotating, primary trailing vortices.

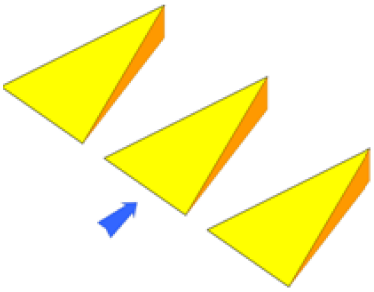

Figure 1. Schematic of an MVG array.

Babinsky et al.[33] note that the herringbone pattern fades about two MVG lengths downstream. They suggest that this is due to the primary trailing vortices lifting off the surface from their mutual upwash. Other than the pri-mary trailing vortex pair, Babinsky and coworkers found two further pairs of trailing vortices, a pair shed from the top of the MVG and another from the junction between the slant sides of the MVG and the floor. Finally, Babinsky et al.,[33] suggest that there is a small separation around the trailing edge of the ramp although this statement appears incomplete.

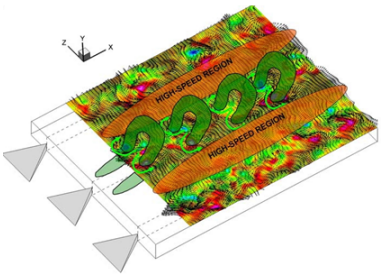

Figure 2. Conceptual sketch of flow downstream of an MVG array, showing the presence of hairpin vortices.

Recently, Blinde et al.,[38] through detailed stereoscopic particle image velocimetry, proposed a model shown in Fig. 2. The figure shows hairpin vortices streaming downstream from each MVG. A high-speed region exists between the streaming hairpin vortices. These observations appear to confirm the observation by Babinsky et al. that the primary trailing vortices lift off the surface which, as suggested by Blinde et al., lead to form hairpin vortices.

Most recently, Li and Liu[41,42] using high-order, large eddy simulations, found a complex flowfield arising from the MVG. First, other than the horseshoe vortex, a number of trailing vortices which then suffer a Kelvin–Helmholtz-like breakdown to form vortex rings, which then propagate to a downstream shock/boundary-layer interaction region. This discovery of vortex rings may be considered to be a further refinement of Blinde et al.'s[38] discovery and awaits experimental confirmation.

II. Experiment

A. Facility and Test Hardware

For brevity, only a summary of the experiments are provided with details available in [43]. The experiments were performed in a blowdown wind tunnel at a Mach number of 2.47 ± 0.005. The tunnel operation was controlled by a host computer which opened the control valve to reach steady-state pressure conditions in about 2–3 s. The total pressure was kept at 517 ± 6 kPa (75 ± 0.9 psia). The duration of the flow visualization experiments was approximately 30s long which resulted in a total temperature drop of only about 1–2 K. Thus, despite the blowdown nature of the tunnel, the temperature can be considered to be steady for the present series of experiments. Thus, the unit Reynolds number can also be considered to be steady at 43 million per m.

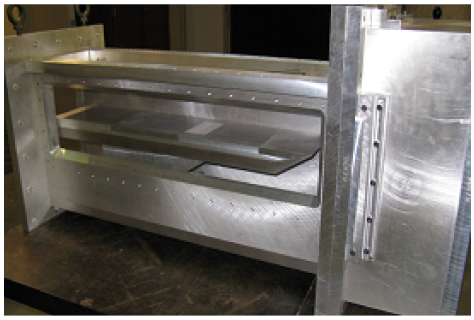

Figure 3. Test section showing flat plate. Flow from right to left.

The test section was 15.2 cm^2 × 81.28 cm long (6 in.^{2} × 2.67 ft). It was outfitted with extensive optical access from

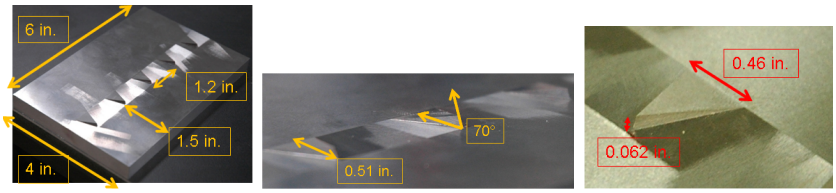

Figure 4. Micro-vortex generator array.

both sides and from the top. A flat plate, 73 cm long (28.75 in), with a sharp leading edge of 15 deg was mounted in the test section[44] over which a boundary layer was developed naturally (Fig. 3). The flat plate was made in layers supported by a sharp tipped rail on each side. The top layer which formed the test surface was made of a number of small, thin plates. These plates butt tightly against each other to form a continuous, flat surface. This modular design allowed for quick configuration changes. A cavity below the top surface allowed pressure tubing, transducer wiring and other elements to be placed. The wiring and tubing were channeled to the rear, either from the side of the test section or from the side of the diffuser, to outside the wind tunnel. A bottom surface encases the cavity.

A micro-vortex generator (MVG) array was mounted with the leading edge located 272 mm (10.7 in.) downstream of the leading edge of the flat plate. Figure 4 shows the array of five MVGs. Each MVG was 12.95 mm (0.51 in.) long and 1.57 mm (0.062 in.) high. The front of the MVG was 11.7 mm (0.46 in.) wide. The center-to-center spacing between the MVGs was 30.5 mm (1.2 in.). Two styles of MVGs were fabricated based on the designs from [42], with the trailing edge angle of either 45 or 70 deg.

III. Particle Image Velocimetry

Particle image velocimetry (PIV) is a quantitative method which uses a combination of a high intensive light source, digital cameras, and seed particles commonly known as tracers to provide an accurate velocity measurement of the flow field being studied. The flow is typically seeded with neutrally buoyant particles which closely represents the fluid. A bright light, such as from a high-powered laser, is then used in conjunction with one or more digital cameras to collect two images with a small separation time dt. These images are then either cross-correlated or auto-correlated and the resulting calculations yield velocity vectors. While the method is fairly sound for subsonic flow, there are concerns that need careful attention when PIV is implemented for supersonic flow.

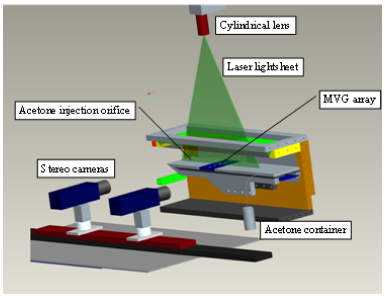

Figure 5. CAD drawing PIV setup configuration

The PIV system utilized in this study includes a New Wave Research Solo 120 double pulse Nd:YAG laser, two LaVision Image Intensive 3S cameras, and DaVis 7.1 Software installed on a computer that houses the Programmable Timing Unit V8. As with most PIV setups, the laser sheet and the cameras are recommended, but not required to be perpendicular with respect to each other. The laser and camera system are mounted on a custom structure attached to Lift Genie model 150. The purpose of the positioning system is to maintain laser and camera alignment. If a different plane is required for collecting data, the entire system can be moved without the need for recalibration.

The optics for the laser has been configured by LaVision to handle two different cylindrical lenses. The divergence of the lens is calculated according to

$$\tan\frac{\alpha}{2} = \frac{d}{2f} \tag{1}$$

With a laser beam diameter of 4.5 mm, the first lens with $f = -10$ mm projects a laser sheet at $\alpha = 24°$. The second lens with $f = -20$ mm projects a laser sheet at 12°.

The FlowMaster 3s Imager Intense cameras capture the images on a CCD chip that is 1376×1040 pixel with a pixel size of 6.45 μm. The scanning rate of the cameras is 16M Hz and they have a maximum readout frequency of 10 fps. For the stereo configuration, two cameras satisfy the Scheimpflug criterion.

If the criterion is not satisfied, the full image will not be in focus and will result in poor calibration. The cameras have a special adapter to allow the correction and satisfy the Scheimpflug criterion. For the stereo configuration, the cameras must also have a viewing angle of at least 10° between the two cameras. The manufacturer recommends the viewing angle to be 30°–45°. For images to be collected the laser and cameras must be synchronized. The synchronization process includes firing the laser, triggering the cameras at two distinct time intervals, transferring data from the cameras to the PIV computer, and resetting the time sequence to restart the process. The PIV system has a dedicated dual processor computer which houses the Programmable Timing Unit V8 that handles the synchronization between the laser and the cameras. While the user has the ability to modify the PTU settings, the manufacturer recommends not to modify the settings and leave them at the optimal default value.

A. Seeding

For fluid flow under supersonic conditions, seed particle characteristics become an important factor. In particular, the density and size of the seed particle have a major influence on seed particle performance. Unlike subsonic flow, seed particles in supersonic flows are exposed to high velocity and density gradients. These gradients greatly affect the momentum of the seed particle and can bring into question the velocity data generated by the correlation equations used by the PIV software. One example of such a situation is when a seed particle crosses a shock wave. Large velocity gradients can cause significant errors due to inertia of the particle when the flow is accelerating or decelerating.[45] Density gradients also produce optical distortions. These distortions are due to nonuniform index refractions and can skew the correlation peak which can have a significant impact on velocity vector calculations.[46] With these known conditions, a suitable seed particle is needed that closely represents the density of fluid being tested. While some error will always remain due to difference in densities between the particle and the fluid, the right seed particle will improve the quality of the data.

For a seed particle to closely represent the characteristics of the surrounding fluid, it is necessary to determine the particle's relaxation time. The particle relaxation time is the time it takes for the particle to respond to the change in conditions of the fluid. The particle relaxation time is calculated using Eqs. 2.

$$\tau = d_p^2 \frac{\rho_p}{18\mu} \tag{2}$$

For a given viscosity the determining factors that effect the particle's relaxation time is the diameter and the density of the particle. As expressed in Eq. 2 the diameter of the seed particle has a more dominate affect due to the square term. Smaller particle diameters will lower the relaxation time meaning quicker response to change in the condition of the fluid. Therefor it is desirable to have the particle's diameter as small as possible.

The density of the particle must take special consideration. For powders granules and other solids, the bulk density is usually given as a property characteristics. For example, the bulk density is defined as the mass of the particles divided by the volume they occupy that includes the space between the particles.[47] This is not the actual density of the individual particle itself. From a molecular standpoint, the molecular mass of the particles are quiet different. The molecular mass of titanium dioxide is less than calcium carbonate leading to the conclusion that titanium dioxide would be a more suitable particle of choice for a given volume, see Table 1. However, the the bulk density for titanium dioxide is greater than the bulk density of calcium carbonate. This contrast can lead to some confusion on which is more suitable as a seed particle. A possible reason for this confusion can be found in the molecular structure. To clarify the confusion it is recommended that the density reference based on x-ray crystallographic data where the density is calculated as the material is in a crystalline structure where voids between individual particles are removed.[48]

Also listed in Table 1 are two liquids; acetone and olive oil. Liquid seed particle have special benefits over solid particles. Solid particles have the ability to remain stable during high fluctuations of temperature and pressures, but have larger diameters and are more dense which increases the particle relaxation time. Liquid particles will have smaller diameters and are less dense which decrease particle relaxation time, but are more sensitive to the changing pressures and temperatures of the surrounding fluid. In this study solid seed particle was chosen to seed the freestream fluid flow while a liquid was used to seed the boundary layer of the flat plate. The injection of the solid seed particles were injected upstream of the test section while the liquid particles were injected from the surface of the flat plate. The solid and liquid particles chosen for the

Table 1. Data on selected seed particles

Seed Name	Chemical Formula	Molecular Weight (g/mol)	ρ_{bulk} (g/cm^3)	X-ray (g/cm^3)	τ $\left(10^{-6}\right)$ s
Calcium carbonate	$CaCO_3$	100.09	0.7	2.71	4.809
Sodium Bicarbonate	$CHNaO_3$	84.01	0.8	2.159	3.697
Graphite	C	12.01	0.77	2.267	3.857
Titanium dioxide	TiO_2	79.86	0.77	3.8-4.1	7.197
Calcium sulfate	CaO_4S	136.17	0.72	2.964	3.947
Olive oil	$C_{19}H_{22}O_6$	346.37	0.8-0.9	–	1.555
Acetone	C_3H_6O	58.08	0.784	–	1.347

current experiments was calcium carbonate with a particle size of .7μm and acetone. The conditions inside the test section are such that acetone existed naturally as a vapor, however the acetone for the experiments was naturally aspirated into the test section as a liquid. Although not verified during experimental testing, it is reasonable to concluded from image results that under the combination of low pressure, low temperature, and high velocity in the test section, acetone is considered to be a wet vapor for the length of the test area.

As stated earlier, the solid seed is injected upstream of the test section. To ensure proper seeding of the entire flow, a seed delivery apparatus must be properly positioned in wind tunnel. Due to the high speeds in the test section, the seeding injection port was located in the plenum chamber just upstream of the windtunnel nozzle. The flow in the plenum chamber is subsonic and is maintained at 75 psig. Previous static tests have concluded that good seeding occurs when the pressure differential is at least 100 psi. Therefore, the seeding apparatus must be able to withstand and maintain a pressure of 175 psig or greater.

The seeder apparatus itself is a cyclone design. A supply of dry compressed air enters the bottom of the seeder through a 5 in. opening. Upon entry into the lower housing, the air is funneled into a 0.5 in. union to the second housing. Once the air enters the main chamber the main chamber, the air is split into two section. The outer section bypasses the seeding chamber and is used to initiate vortex flow near the exit of the seeder. The air in the inner chamber diverges and encounters a 1μm filter. This barrier prevents most of the seed particles from falling to the lower chamber of the seeder. The mixed air and seed particles travel upward through a second 100 μm wire mesh filter and is design to separate large size particles that may have formed. After the final filter, the seeded air is combined with the outer channel where it is mixed using a vortex and then passes through the 0.5 in. exit port. This size of the exit port ensure that the mass flow rate entering the seeder is the same mass flow rate exiting the seeder. The seeded air is then piped into the plenum chamber where it was injected into the freestream. The dry air that feeds the seeder was controlled remotely using a McMaster-Carr Model 4738K502 energy efficient Buna-N diaphram brass solenoid valve and the valve control computer which operated the windtunnel.

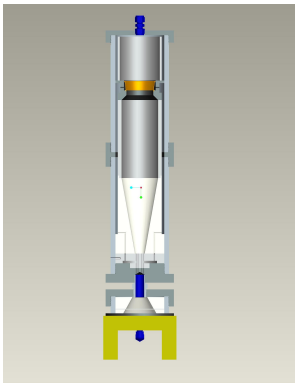

Figure 6. CAD drawing of seeder apparatus.

B. Surface Reflection

A common concern during PIV testing is surface reflection produced by the high intensity laser. The severity of the reflection is influence partially by the material being used, the intensity of the light source, and application of image filtering. The material selected can have a predominant effect on the severity of the surface reflection. Examples of three different surfaces are given in Fig. 7. Figure 7(a) shows the laser impacting the surface of a section of Lexan material. The Lexan polycarbonate allows most of the high intensity light to pass through the surface. Only a small fraction remains and is indicated by the reflection off of particles directly above the light shown in Fig. 7(a). By the time the light reflects off other the lower surfaces, the reflected light is either out of the field of view of the camera or is not in the desired tested region. The reflection seen in Fig. 7(a) is a reflection off the surface which the lexasn lays. For supersonic

boundary layer studies, the insertion of polycarbonate material may result in surface flow influence along the edges. The temperature conditions of the test section must also be considered. Depending on the compound of the Lexan material the subzero temperatures near the brittle point of some polycarbonate compounds. This could make the material more vulnerable to pressure fluctuations.

The optimal case is Fig. 7(b). The back–faced mirror allows the light to pass through the surface and is reflected in the same direction that as it traveled. The only indication of laser contacting the surface are the reflection off of dust particles on the surface of the mirror and along the edges of the mirror itself. However, application of a mirrored surface for supersonic boundary layer flow studies poses it own engineering design challenges.

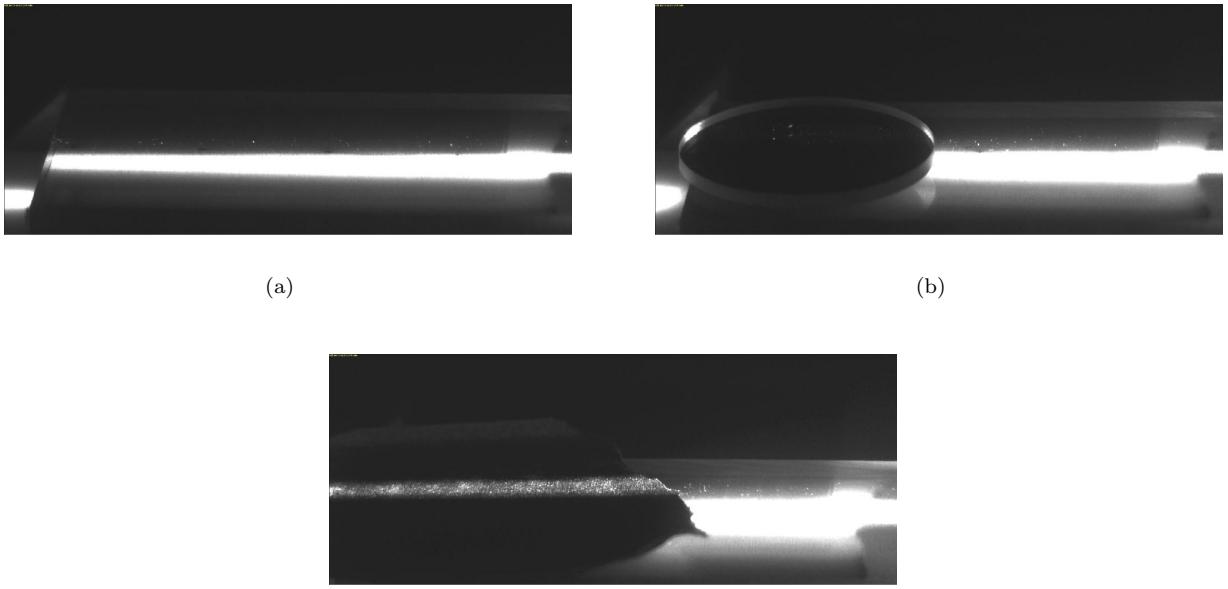

(a) (b)

(c)

Figure 7. Surface reflection demonstration on (a) Lexan (b) Lexan and Mirror (c) Lexan and black paint.

A coat of matte black paint can be applied to the surface to reduce surface reflections without the requirement of major modifications. A example of such an application is shown in Fig. 7(c). While not able to fully eliminate all surface reflection, the application of matte black paint reduces the surface reflection when compared to surface reflection of aluminum.

Surface reflection reduction in the current study involved a combination of surface preparation, laser intensity setting, and camera position. For surface preparation, the first step is to eliminate all surface cracks and imperfections. This was accomplished by applying a thin layer of Bondo, a commonly used filler for body restorations on automobiles. The Bondo is then sanded using an electric sander with up to #220 grit sandpaper. A thin layer of matte black was then sprayed onto the surface.

In addition to the coat of matte black paint, a layer of Dykem Steel Red was applied to the surface. The dye itself appears to have Rhodamine characteristics. Rhodamine is known to be utilized as a dye as well have the ability to absorb wavelength near 530 nm. Different types of rhodamine will have different wavelength absorption properties. The wavelength of the laser is 532 nm which is close to the Rhodamine absorption. Rhodamine itself will dissolve in water or alcohol. Application of either a water- or alcohol-based solutions to an aluminum surface proved to be difficult. It was founded that Dykem Steel Red a solution made up of several alcohols as its base and has a red dye as the color. The exact makeup of the dye is unkown, but test showed to have laser emission absorption characteristics similar to Rhodamine. This dye was applied to the local area where the laser impacts the surface. Surface reflection were further reduced allowing data collection very close to the surface.

The intensity of the laser also impacts surface reflections. If the laser intensity is high, the surface reflection will increase. Therefore the laser must be set to a low intensity value to minimize surface impact

reduce over saturations. Control of laser intensity is handled by the PIV computer.

Camera angle with respect to the surface is the most simplest modification to reduce surface reflections. If the cameras are positioned perpendicular to the image plane, then most of the reflected light wave will be directed away from the camera. If the camera sits too low, the images features closer to the camera will interfere with the image plane of interest. If the cameras is positioned at to high of an angle, the reflections will become more noticable. The optimal angle for the current study was found to be 10°.

IV. Results and Discussion

Preliminary test were first conducted using calcium carbonate and acetone separately. Results for both conditions are shown in Fig. 8. For freestream seeding with calcium carbonate, the tests confirm the effectiveness of the delivery system as well as revealing activity occurring within boundary layer downstream of the MVG. The calcium carbonate seed particles, however, were not able to reveal detailed turbulent flow structure. A reasonable conclusion is the solid seed particle's relaxation time is too high and is not able to react quickly enough to respond to the changing in flow conditions.

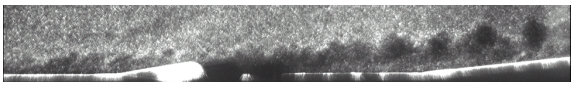

(a)

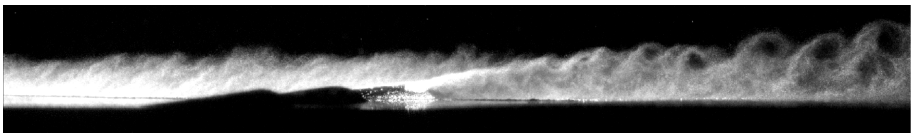

(b)

Figure 8. PIV image result of (a) Calcium carbonate seeding (b) Acetone boundary layer seeding

Figure 8(b) shows the test results using acetone seed being naturally aspirated in the compressible turbulent boundary layer. Turbulent activity and structures are clearly visible downstream of the vortex generators. It is clearly evident that the increase in turbulent structure visualization is due to the particle relaxation time of acetone. Figure 9 shows the overall combination of freestream seeding and boundary layer surface seeding using both calcium carbonate and acetone.

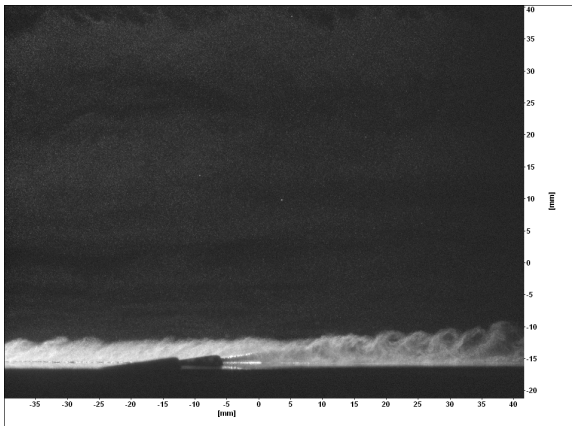

Figure 9. Combination of mixed seeding.

While initial test produce satisfactory results, complication in freestream seeding did arise. Pressure

requirements for the seeder could only be maintained for approximatly 6s . After that time, the seed dispersion became erratic and non–uniformed. The images collected with good seed dispersion were similiar to Fig. 9. Freesteam velocity and Mach number was verified using Schlieren imagery.

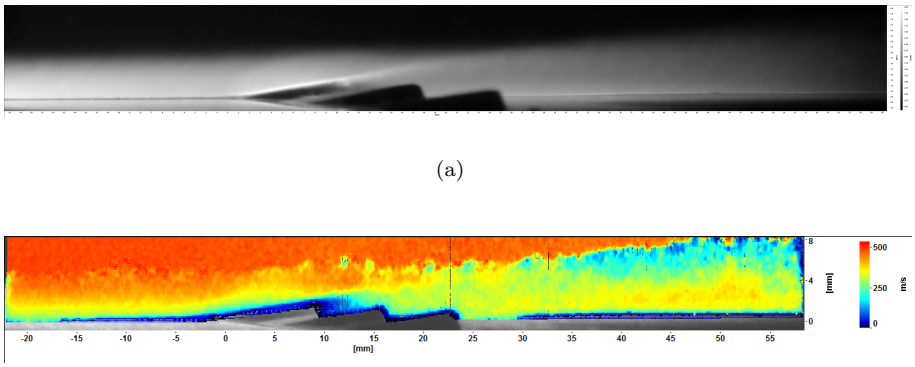

Figure 10. PIV data collection results (a) Time-averaged image profile (b) Time-average vector calculations

Figure 10(a) and Figure 10(b) show the results of the piv data collected. Figure 10(a) is a compiled average of images collected for one particular test configuration. While not visible in the figure, the boundary layer thickness upstream of the MVG is approximately 4 mm[43] as expected for a flat plate at Mach 2.47. Figure 10(b) is the results for time-averaged vector calculations for the same configuration. The effects of the MVGs on the compressible turbulent boundary layer are clearly evident in both images. The time-average velocity profiles are calculated from approximately 125 images. The amount of data collected was limited by the PIV system performance and windtunnel operation time.

Results from PIV data were it is exported as .dat format and imported into Mathematica were boundary layer calculation were calculated according to Ref. [43]. Figure 11 represents the upstream profile at several locations for the one MVG configuration. The results agreed well with theory.

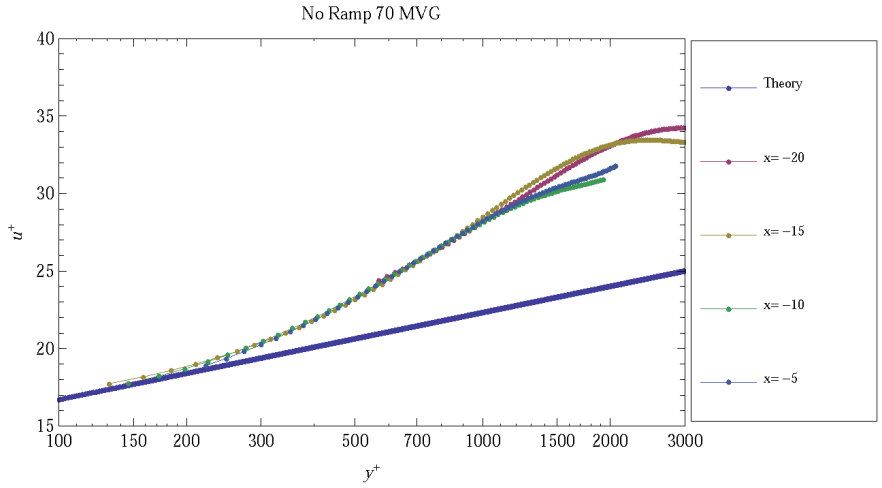

Figure 11. Boundary layer profile upstream MVG.

Due to the complication involving longer term freestream seeding, the average freestream velocity data collected was consider not reliable for most of images. The acetone seed work well in capturing most of the boundary layer characteristics down to approximately $y^+ = 200$. Calculations below this value were disregarded due to accuracy uncertainty. The reason for the sudden stop was an severe effect of the acetone on the surface paint. While there were expectations of paint stripping, the severity of the data corruption

was unexpected. For some configurations data below $y^+ = 200$ agreed well with theory, however in other cases the results did not agree. It was later determined that below $y^+ = 200$ agreement with theory only occurred when the kinematic viscosity was changed from air to an average of air and acetone indicating a possibility that either the flow was over saturated or a direct influence of the paint stripping from the surface.

V. Conclusions

For the current study a new seeding and surface treatment method was conducted. A combination of surface flow preparations, laser light intensity settings and camera positioning was implemented. The optimal surface was determined to be a back-faced mirror surface while the application of matte black paint proved to be the most practical for aluminum surfaces. The application of Dykem Steel Red showed to have Rhodamine properties further reducing surface reflections. Camera positioning and laser intensity also improve the images due to the influence of surface reflections.

For turbulent boundary layer seeding acetone was naturally aspirated into the boundary layer. The freestream was seeded using calcium carbonate. The result concluded the necessity for selecting the right seed particle for the right conditions. Determine the correct seed particle was determined by the particle relaxation time which is influenced by the particle's diameter and density using X-Ray crystallograph. The results revealed complex flow structures influenced by the MVG's. The combination of freestream seeding using calcuim carbonate and surface flow seeding using acetone proved multiple seed test can be performed and be utilized effectively.

Acknowledgments

The authors gratefully acknowledge funding for this work via AFOSR Grant No. FA9550-08-1-0201 monitored by Dr. John Schmisseur. The authors thank the assistance of Rod Duke, Yusi Shih and David Whaley with the experiments. David Whaley was supported by a High School Research Internship under a Texas Youth in Technology grant from the Texas Workforce Commission, administered by Dr. J. Carter M. Tiernan. The authors thank Richard R. Mitchell for designing the cyclone seeder.

References

[1]Raffel, M., Willert, C., Wereley, S., and Kompenhans, J., *Particle Image Velocimetry: A Practical Guide*, Springer, Berlin, 2nd ed., 2007.

[2]Merzkirch, W., *Flow Visualization*, Academic Press, Orlando, 1987.

[3]Lu, F. K., Pierce, A. J., and Shih, Y., "Experimental Study of Near Wake of Micro Vortex Generators in Supersonic Flow," AIAA Paper 2010–4623, 2010.

[4]Holmes, A. E., Hickey, P. K., Murphy, W. R., and Hilton, D. A., "The Application of Sub-Boundary Layer Vortex Generators to Reduce Canopy 'Mach Rumble' Interior Noise on the Gulfstream III," AIAA Paper 1987–0084, 1987.

[5]Lin, J. C., McGhee, S. K., and Valarezo, W. O., "Separation Control on High-Lift Airfoils via Micro-Vortex Generators," *Journal of Aircraft*, Vol. 31, No. 6, 1994, pp. 1317–1323.

[6]Lin, J. C., "Control of Turbulent Boundary-Layer Separation Using Micro-Vortex Generators," AIAA Paper 1999-3404, 1999.

[7]Ashill, P. R., Fulker, J. L., and Hackett, K. C., "Research at DERA on Sub Boundary Layer Vortex Generators (SBVGs)," AIAA Paper 2001–0887, 2001.

[8]Allan, B. G., Yao, C.-S., and Lin, J. C., "Numerical Simulations of Vortex Generator Vanes and Jets on a Flat Plate," AIAA Paper 2002–3160, 2002.

[9]Ashill, P. R., Fulker, J. L., and Hackett, K. C., "Studies of Flows Induced by Sub Boundary Layer Vortex Generators (SBVGs)," AIAA Paper 2002–0968, 2002.

[10]Jenkins, L. N., Gorton, S. A., and Anders, S. G., "Flow Control Device Evaluation for an Internal Flow with an Adverse Pressure Gradient," AIAA Paper 2002–0266, 2002.

[11]Lin, J. C., "Review of Research on Low-Profile Vortex Generators to Control Boundary-Layer Separation," *Progress in Aerospace Science*, Vol. 38, No. 4–5, 2002, pp. 389–420.

[12]Patel, M. P., Carver, R., Lisy, F., Prince, T. S., and Ng, T., "Detection and Control of Flow Separation Using Pressure Sensors and Micro-Vortex Generators," AIAA Paper 2002–0268, 2002.

[13]Patel, M. P., Prince, T. S., Carver, R., DiCocco, J. M., Lisy, F. J., and Ng, T. T., "Deployable Flow Effectors for Phantom Yaw Control of Missiles at High Alpha," AIAA Paper 2002–2827, 2002.

[14]Patel, M. P., Prince, T. S., Carver, R., DiCocco, J. M., Lisy, F. J., and Ng, T. T., "Control of Aircraft Stall via Embedded Pressure Sensors and Deployable Flow Effectors," AIAA Paper 2002–3170, 2002.

[15]Rae, A. J., Galpin, S. A., and Fulker, J., "Investigation into Scale Effects on the Performance of Sub Boundary-Layer Vortex Generators on Civil Aircraft High-Lift Devices," AIAA Paper 2002–3274, 2002.

[16]Tai, T. C., "Effect of Midwing Vortex Generators on V-22 Aircraft Forward-Flight Aerodynamics," *Journal of Aircraft*, Vol. 40, No. 4, 2003, pp. 623–623.

[17]Jirásek, A., "A Vortex Generator Model and its Application to Flow Control," AIAA Paper 2004–4965, 2004.

[18]Osborn, R. F., Kota, S., Hetrick, J. A., Geister, D. E., Tilmann, C. P., and Joo, J., "Active Flow Control Using High-Frequency Compliant Structures," *Journal of Aircraft*, Vol. 41, No. 3, 2004, pp. 603–609.

[19]Wik, E. and Shaw, S. T., "Numerical Simulation of Micro Vortex Generators," AIAA Paper 2004–2697, 2004.

[20]Ahmad, K. A., McEwan, W. T., Watterson, J. K., and Cole, J. S., "Numerical Study of a Vibrating Sub-Boundary Layer Vortex Generator," AIAA Paper 2005–4648, 2005.

[21]Ahmad, K. A., McEwan, W. T., Cole, J. S., and Briggs, I., "Sub-Boundary Layer Vortex Generator Control of a Separated Diffuser Flow," AIAA Paper 2005–4650, 2005.

[22]Jirásek, A., "Vortex-Generator Model and Its Application to Flow Control," *Journal of Aircraft*, Vol. 42, No. 6, 2005, pp. 1486–1491.

[23]Bohannon, K. S., "Passive Flow Control on Civil Aircraft Flaps Using Sub-Boundary Layer Vortex Generators in the AWIATOR Programme," AIAA Paper 2006–2858, 2006.

[24]Jirásek, A., "Development and Application of Design Strategy for Design of Vortex Generator Flow Control in Inlets," AIAA Paper 2006–1050, 2006.

[25]Anderson, B. H., Tinapple, J., and Sorber, L., "Optimal Control of Shock Wave Turbulent Boundary Layer Interactions Using Micro-Array Actuation," AIAA Paper 2006–3197, 2006.

[26]Babinsky, H., Makinson, N. J., and Morgan, C. E., "Micro-Vortex Generator Flow Control for Supersonic Engine Inlets," AIAA Paper 2007–2007, 2007.

[27]Holden, H. and Babinsky, H., "Effect of Microvortex Generators on Separate Normal Shock/Boundary Layer Interactions," *Journal of Aircraft*, Vol. 44, No. 1, 2007, pp. 89–96.

[28]Shinn, A. F., Vanka, S. P., Mani, M., Dorgan, A., and Michal, T., "Application of BCFD Unstructured Grid Solver to Simulation of Micro-Ramp Control of Shock/Boundary Layer Interactions," AIAA Paper 2007–3914, 2007.

[29]Babinsky, H. and Ogawa, H., "SBLI Control for Wings and Inlets," *Shock Waves*, Vol. 18, No. 2, 2008, pp. 89–96.

[30]Ghosh, S., Choi, J.-I., and Edwards, J. R., "RANS and Hybrid LES/RANS Simulation of the Effects of Micro Vortex Generators Using Immersed Boundary Methods," AIAA Paper 2008–3728, 2008.

[31]Meunier, M. and Brunet, V., "High-Lift Devices Performance Enhancement Using Mechanical and Air-Jet Vortex Generators," *Journal of Aircraft*, Vol. 45, No. 6, 2008, pp. 2049–2061.

[32]Anderson, B. H., Mace, J. L., and Mani, M., "Active `Fail Safe' Micro-Array Flow Control For Advanced Embedded Propulsion Systems," AIAA Paper 2009–0920, 2009.

[33]Babinsky, H., Li, Y., and Pitt Ford, C. W., "Microramp Control of Supersonic Oblique Shock-Wave/Boundary-Layer Interactions," *AIAA Journal*, Vol. 47, No. 3, 2009, pp. 668–675.

[34]Domel, N. D., Baruzzini, D., and Miller, D. N., "CFD Results for Shock-Boundary Layer Flow Control with Micro-Ramps at Various Grid Densities," AIAA Paper 2009–4016, 2009.

[35]Galbraith, M. C., Orkwis, P. D., and Benek, J. A., "Multi-Row Micro-Ramp Actuators for Shock Wave Boundary-Layer In-teraction Control," AIAA Paper 2009–0321, 2009.

[36]Lee, S., Loth, E., Georgiadis, N. J., and DeBonis, J. R., "Effect of Mach Number on Flow Past Micro-Ramps," AIAA Paper 2009–4181, 2009.

[37]Rybalko, M., Loth, E., Chima, R. V., Hirt, S. M., and DeBonis, J. R., "Micro-Ramps for External Compression Low-Boom Inlets," AIAA Paper 2009–4206, 2009.

[38]Blinde, P. L., Humble, R. A., van Oudheusden, B. W., and Scarano, F., "Effects of micro-ramps on a shock wave/turbulent boundary layer interaction," *Shock Waves*, Vol. 19, No. 6, 2009, pp. 507–520.

[39]Bur, R., Coponet, D., and Carpels, Y., "Separation Control by Vortex Generator Devices in a Transonic Channel Flow," *Shock Waves*, Vol. 19, No. 6, 2009, pp. 521–530.

[40]Lee, S., Goettke, M. K., Loth, E., Tinapple, J., and Benek, J., "Microramps Upstream of an Oblique-Shock/Boundary-Layer Interaction," *AIAA Journal*, Vol. 48, No. 1, 2010, pp. 104–118.

[41]Li, Q. and Liu, C., "LES for Supersonic Ramp Control Flow Using MVG at $M = 2.5$ and $Re_\theta = 1440$," AIAA Paper 2010–0592, 2010.

[42]Li, Q. and Liu, C., "Numerical Investigation on the Effects of the Declining Angle of the Trailing Edge of MVG," AIAA Paper 2010–0714, 2010.

[43]Pierce, A. J., *Experimental Study of Micro-Vortex Generators at Mach 2.5*, MSAE thesis, University of Texas at Arlington, 2010.

[44]Mitchell, R. R. and Lu, F. K., "Development of a Supersonic Aerodynamic Test Section using Computational Modeling," AIAA Paper 2009–3573, 2009.

[45]Tedeschi, G., Gouin, H., and Elena, M., "Motion of Tracer Particles in Supersonic Flows," *Experiments in Fluids*, Vol. 26.

[46]Scarano, F., "Overview of PIV in Supersonic Flow," *Topics Applied Physics*, Vol. 112, 2008, pp. 445–463.

[47]ASTM, "Standard Test Method for Real Density of Calcined Petroleum Coke by Xylene," 1999, pp. 5–8.

[48]Weast, R., *CRC Handbook of Chemistry and Physics*, CRC Press, 1988.